TERRESTRIAL EVAPORATION RESPONSE TO MODES OF CLIMATE VARIABILITY

SUPPLEMENTARY MATERIAL

Martens et al., 2018

1. SUPPLEMENTARY METHODS
EVAPORATION DATASET

To increase the robustness of our results, three global and observation-based datasets of terrestrial evaporation were selected here: (1) the Global Land Evaporation Amsterdam Model (GLEAM) v3.1a dataset [1,2], (2) the Penman–Monteith–Leuning dataset [3], and (3) the FLUXNET Model Tree Ensemble (MTE) dataset [4,5]. The de-trended, standardized anomalies of the three datasets of terrestrial evaporation (Method Section of main manuscript) are merged at the pixel level based on their relative errors:

$$E_{\mathrm{mrg}}^{t} = \sum_{i=1}^{3} w_i E_i^t$$

where E_{mrg}^{t} is the merged estimate at time t, E_i^t the estimate of terrestrial evaporation from dataset i at the same time, and w_i the relative weight calculated using the standard deviation of the error distributions at the pixel level:

$$w_i = \frac{{\sigma_i}^{-1}}{\sum_{j=1}^{3} {\sigma_j}^{-1}}$$

where σ_i is the standard deviation of the error distribution of dataset i. The latter is calculated using a Triple Collocation Analysis (TCA) [6], with the GLEAM v3.1a dataset as a reference. The TCA is applied on the pixel-based anomaly time series of terrestrial evaporation (for the period 1982–2012) to obtain spatially distributed weights (Supplementary Fig. 16). Note that the TCA is applied over the entire study period to keep a sufficient number of data samples per pixel [6], resulting in temporally constant weights.

2. SUPPLEMENTARY FIGURES

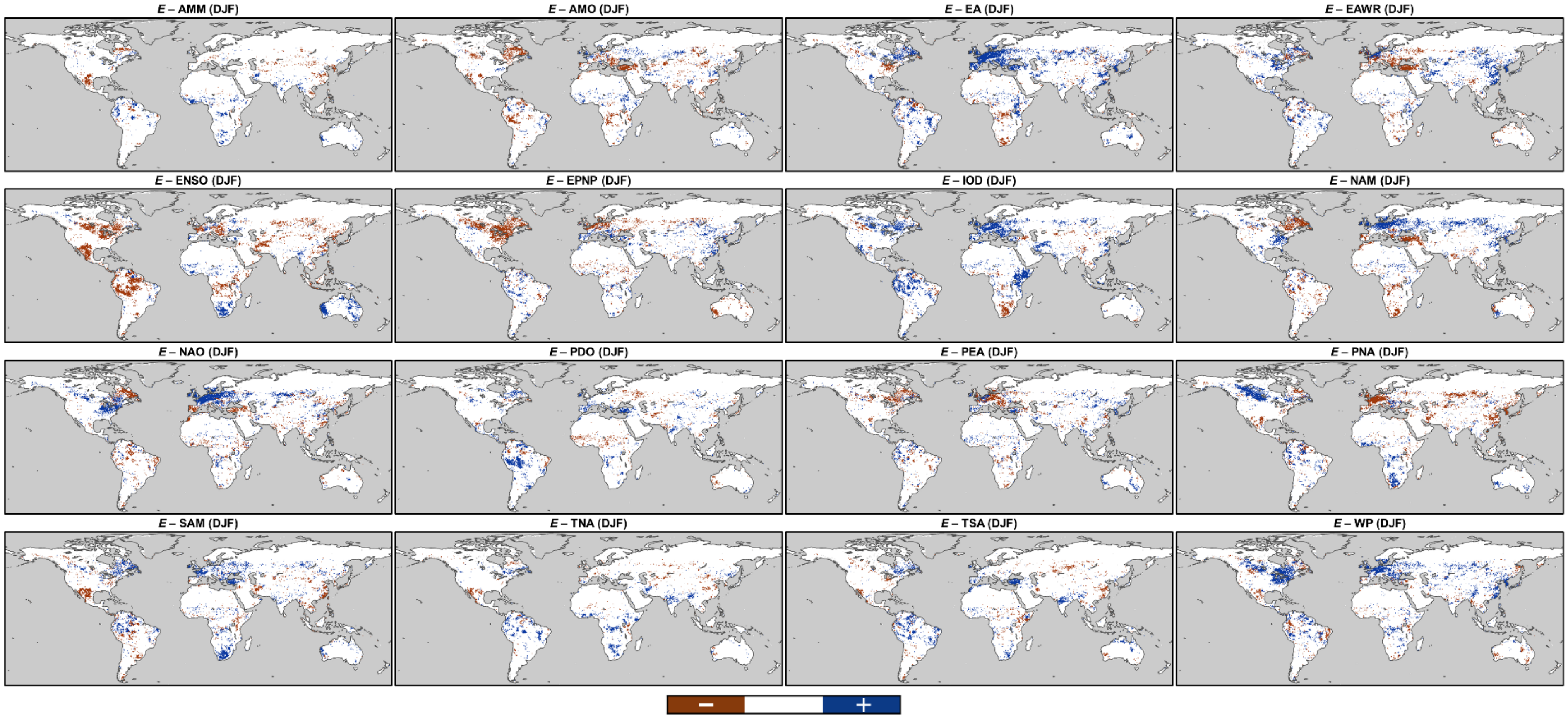

Supplementary Figure 1: Impact of teleconnections on the dynamics of terrestrial evaporation for DJF. Maps display the regions where the mode of variability affects terrestrial evaporation (i.e. the corresponding CI has a regression coefficient > 0 in the LASSO model), and the sign indicates the direction of the relation between the CI, and the variability in terrestrial evaporation. Regression coefficients corresponding to different lags introduced in each CI were summed to assess the overall impact per CI.

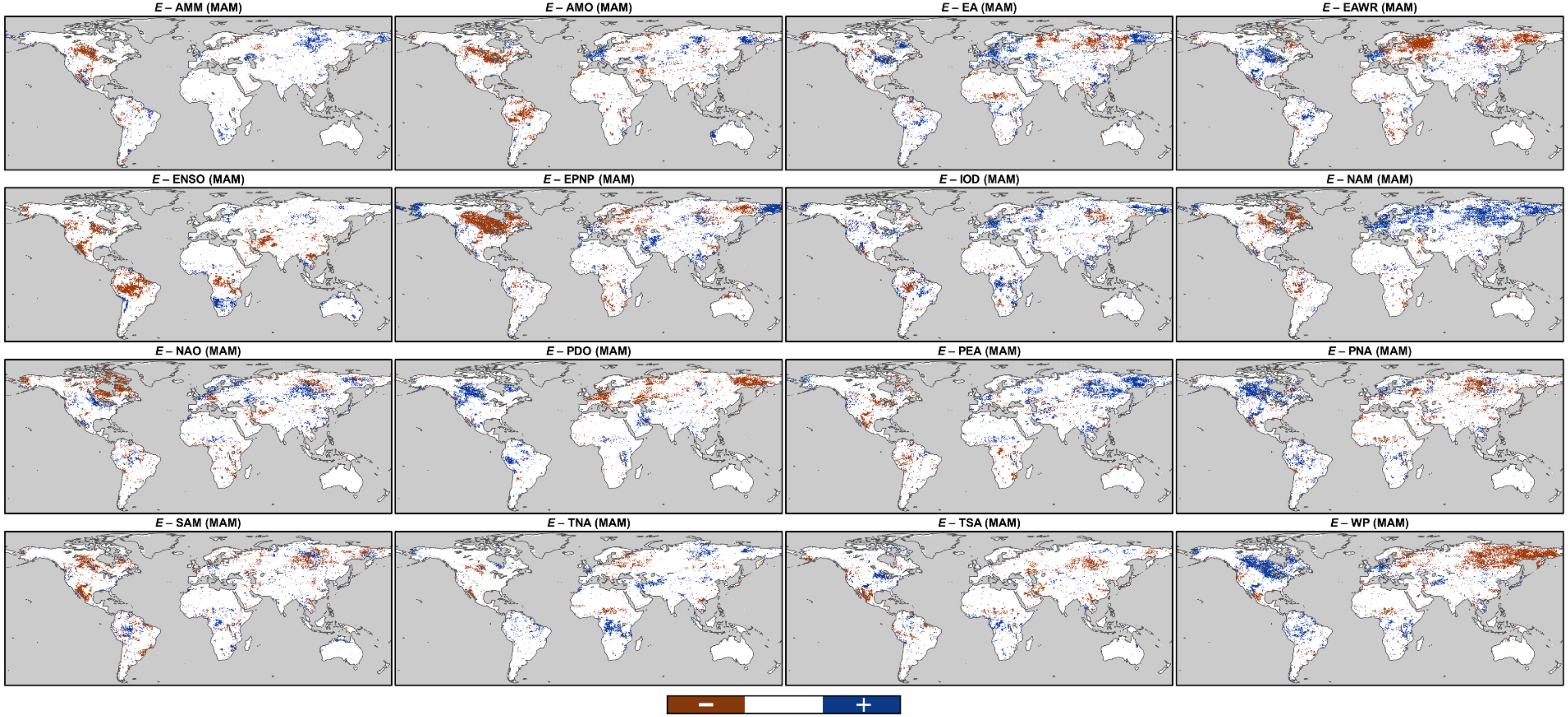

Supplementary Figure 2*:* Like Supplementary Figure 1, but for MAM.

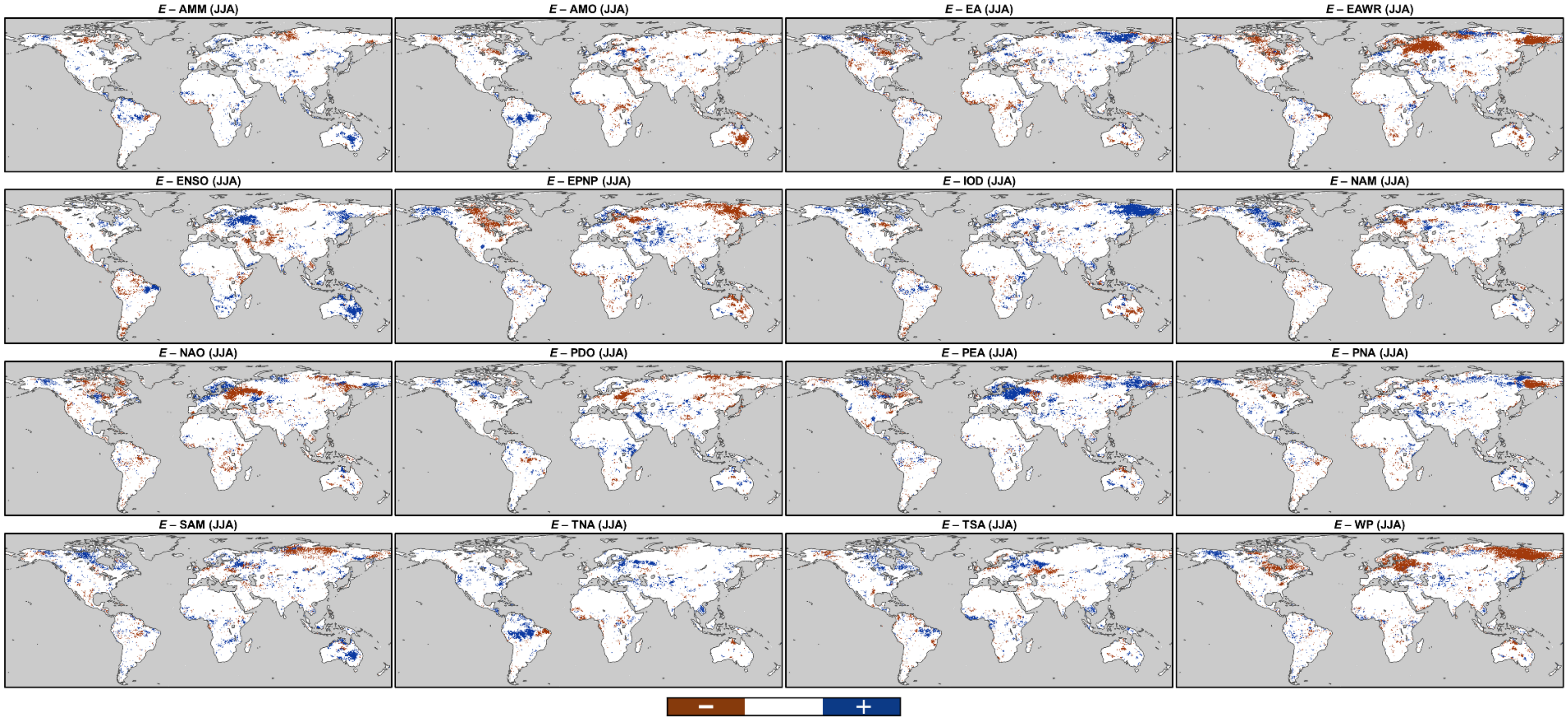

Supplementary Figure 3: Like Supplementary Figure 1, but for JJA.

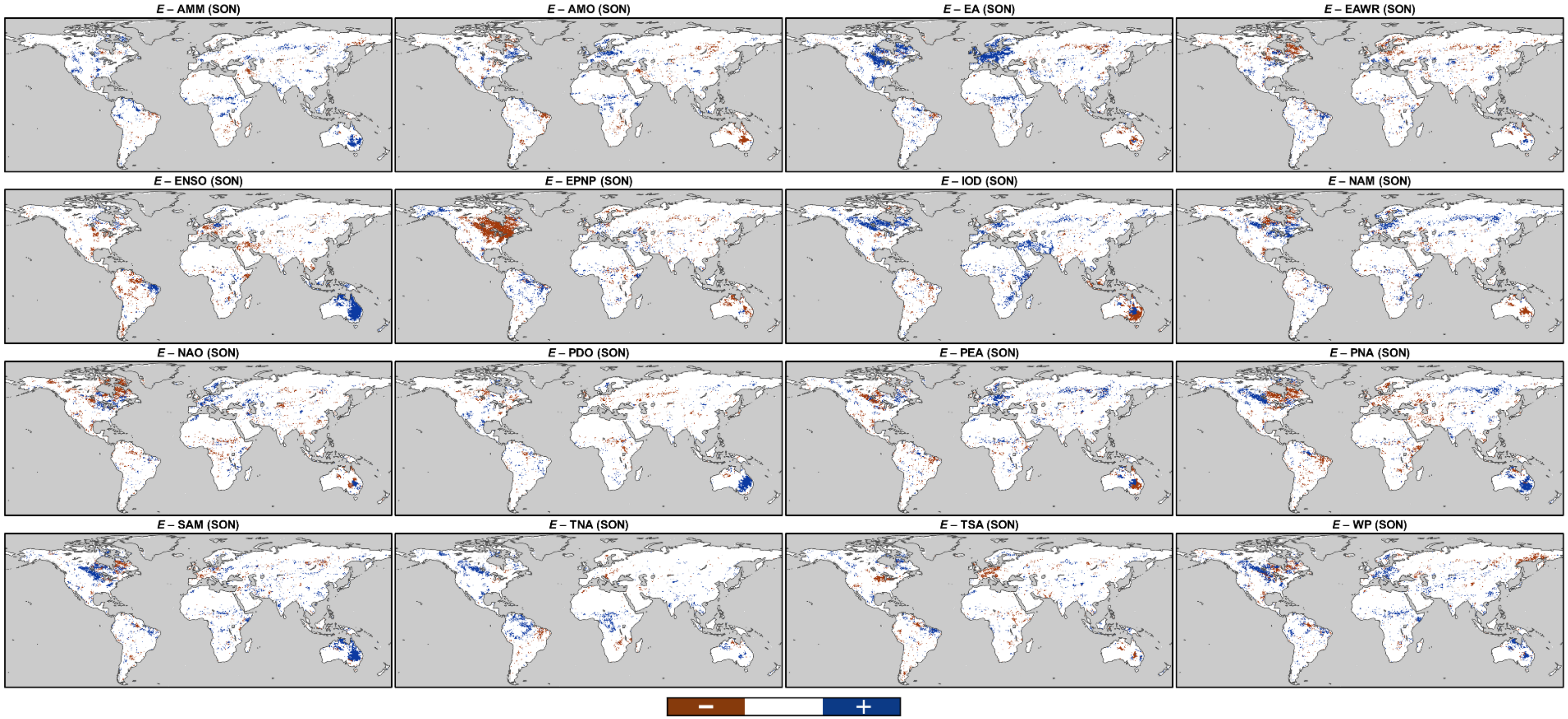

Supplementary Figure 4: Like Supplementary Figure 1, but for SON.

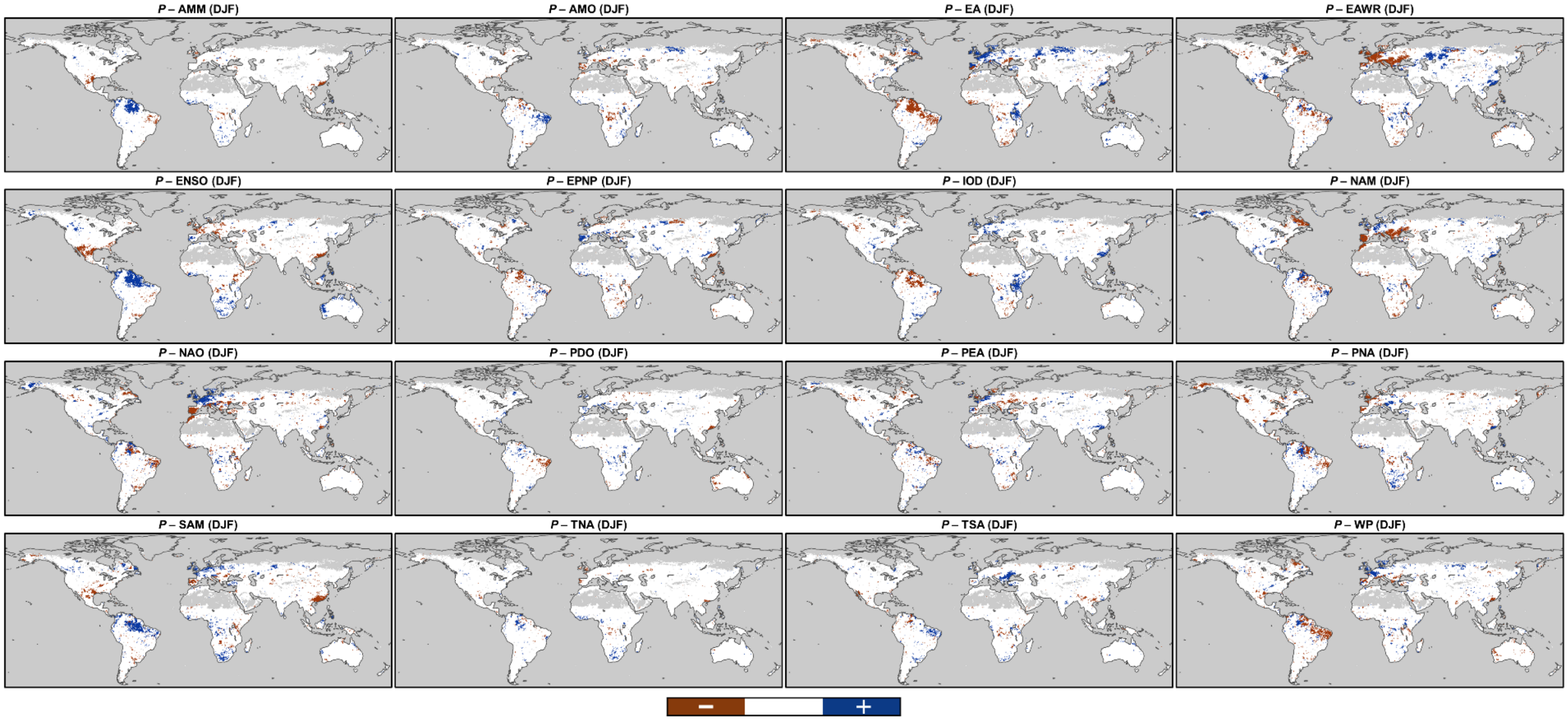

Supplementary Figure 5: Like Supplementary Figure 1, but for precipitation.

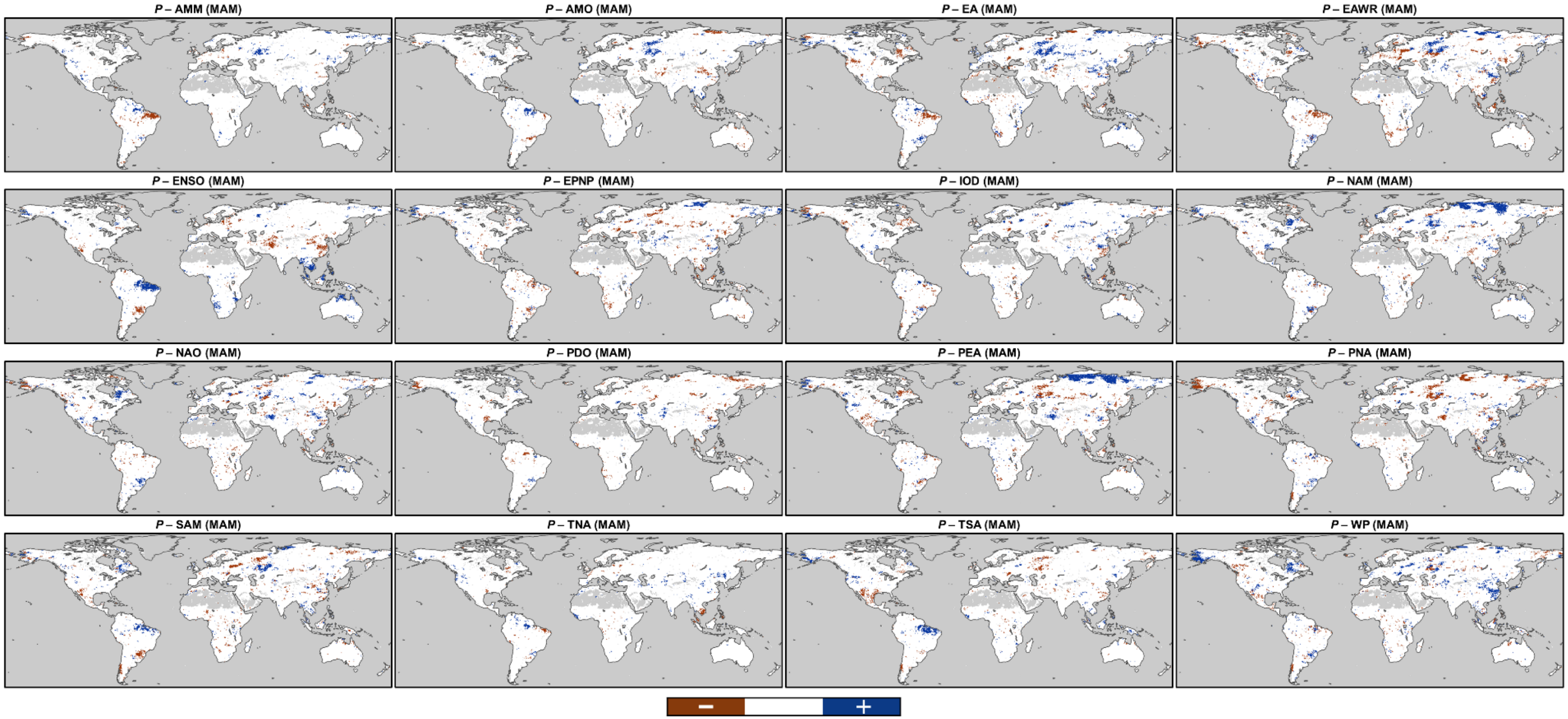

Supplementary Figure 6: Like Supplementary Figure 5, but for MAM.

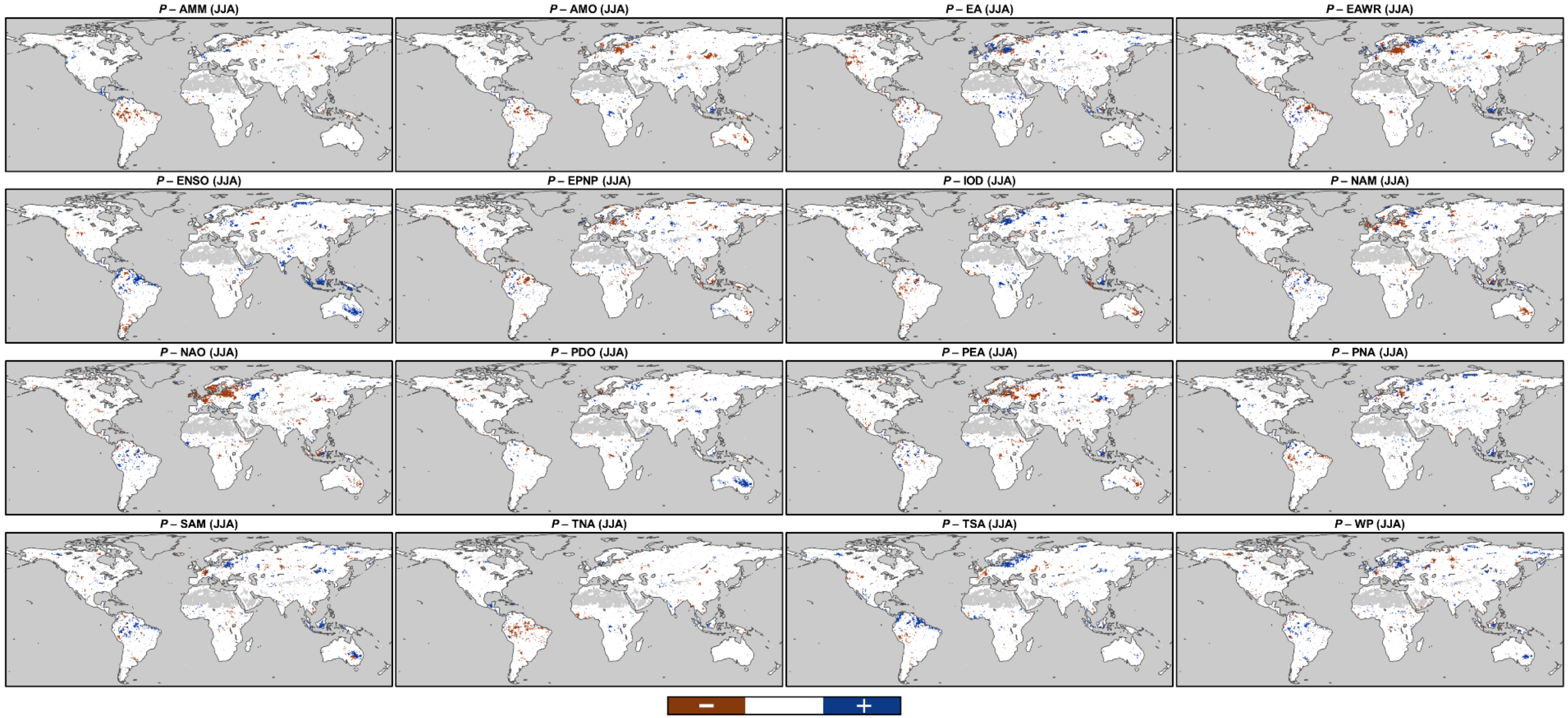

Supplementary Figure 7: Like Supplementary Figure 5, but for JJA.

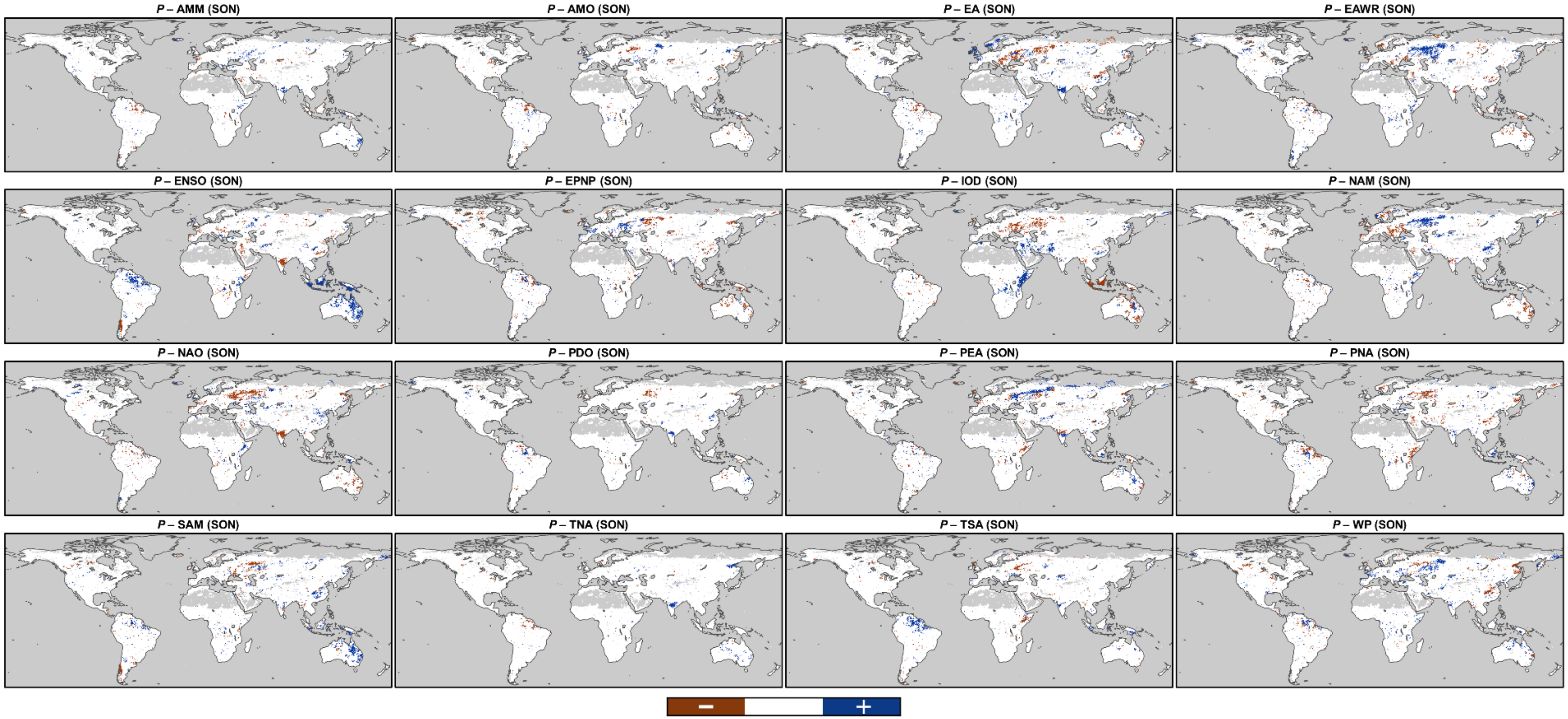

Supplementary Figure 8: Like Supplementary Figure 5, but for SON.

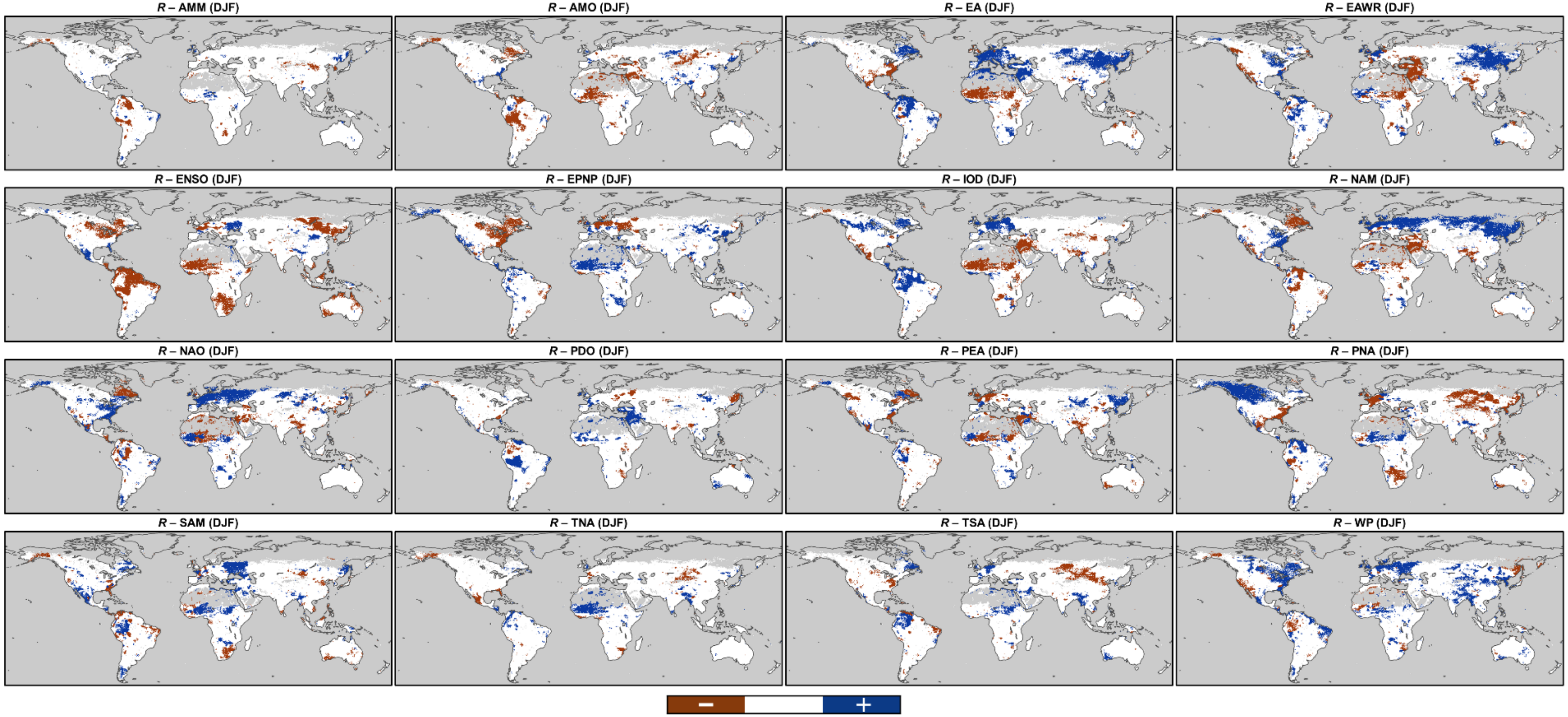

Supplementary Figure 9: Like Supplementary Figure 1, but for total incoming radiation.

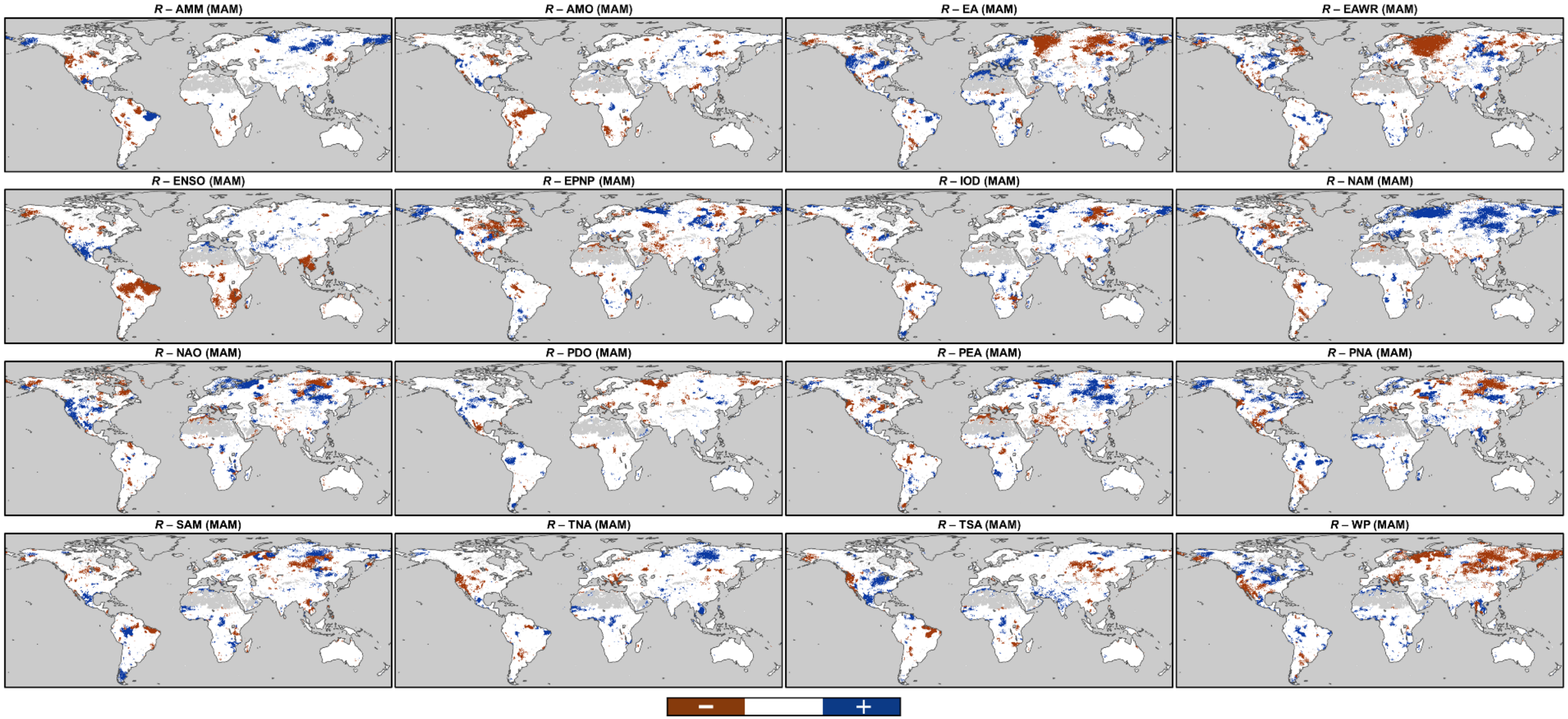

Supplementary Figure 10: Like Supplementary Figure 9, but for MAM.

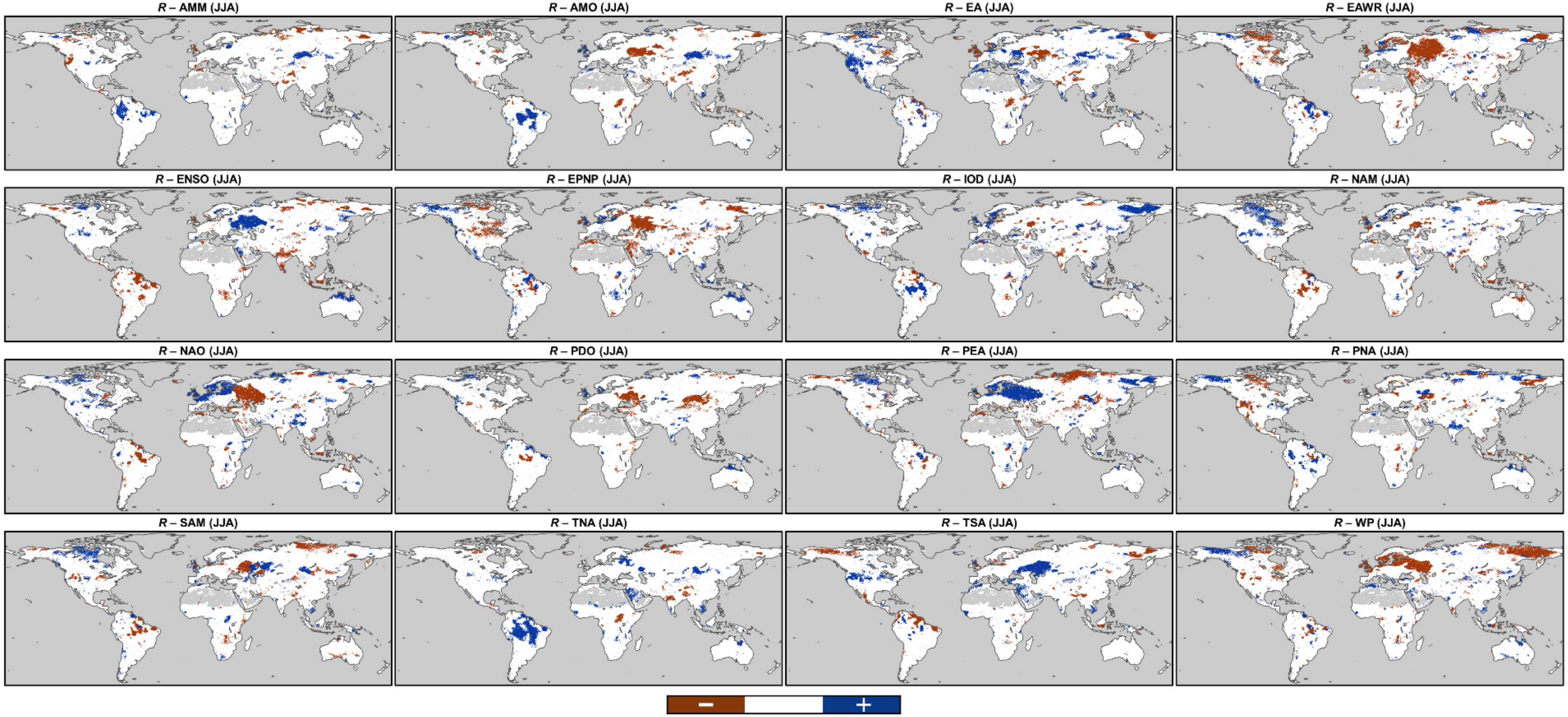

Supplementary Figure 11: Like Supplementary Figure 9, but for JJA.

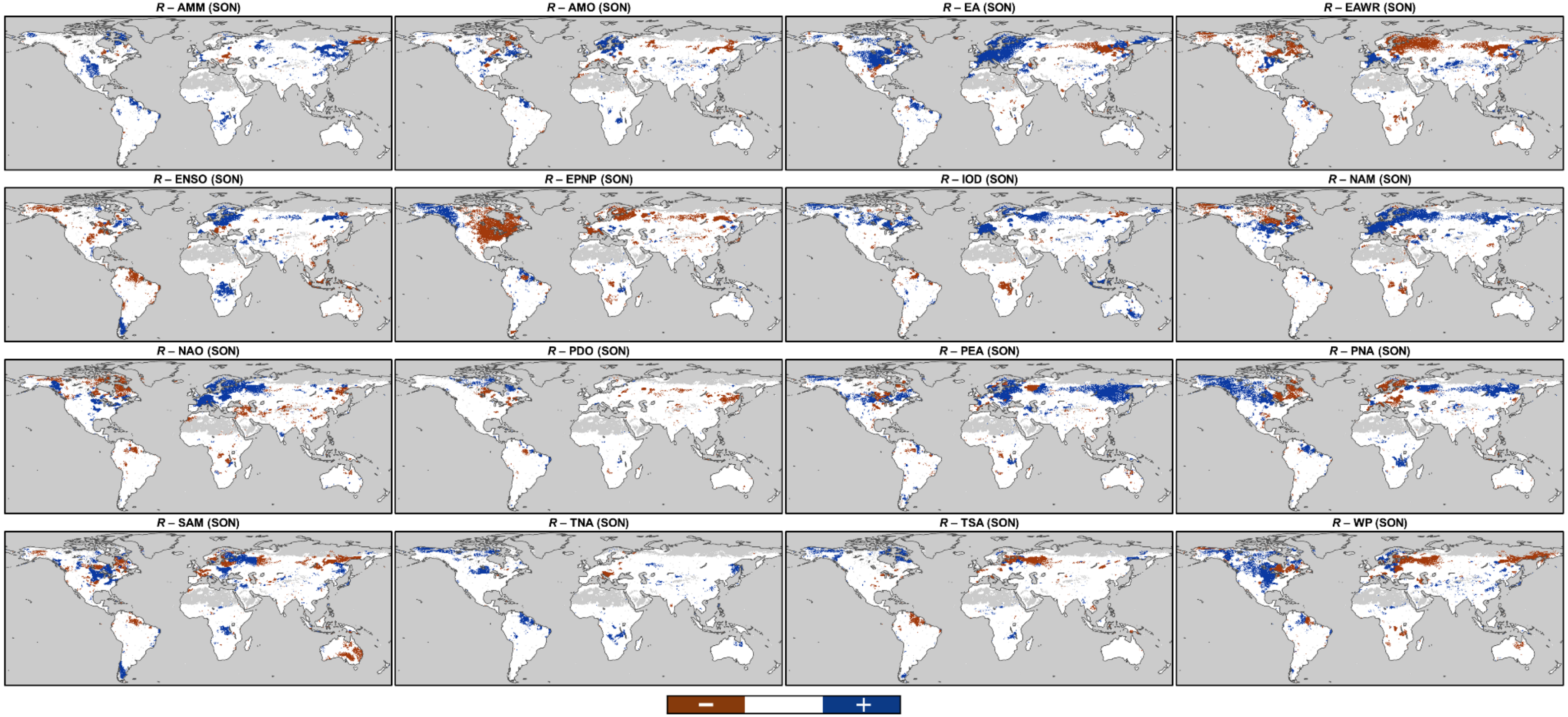

Supplementary Figure 12: Like Supplementary Figure 9, but for SON.

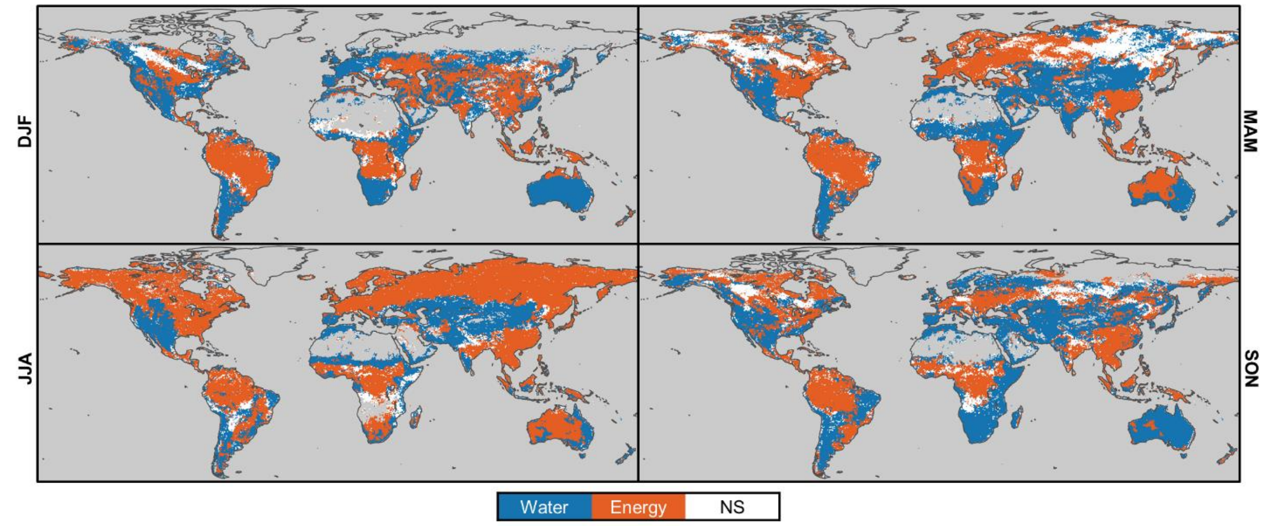

Supplementary Figure 13: Primary drivers of terrestrial evaporation. Classification is obtained by ranking the regression coefficients from the LASSO model targeting the anomalies of terrestrial evaporation based on the anomalies of precipitation and net radiation. Pixels where the regression coefficient for precipitation is top-ranked are classified as water-driven, whereas pixels where the regression coefficient for radiation is top-ranked are classified as energy-driven. NS indicates non-significant pixels.

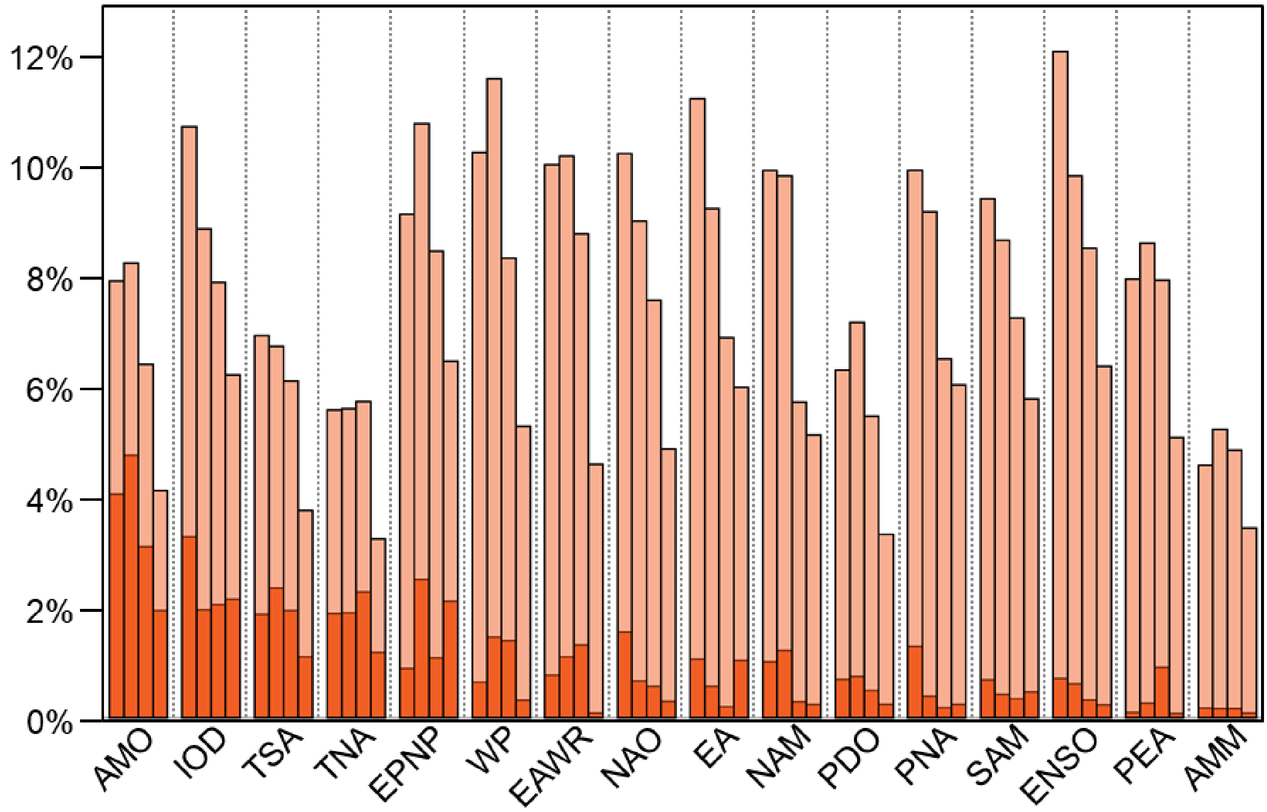

Supplementary Figure 14: Like Fig. 3, but percentages for both Hemispheres summed.

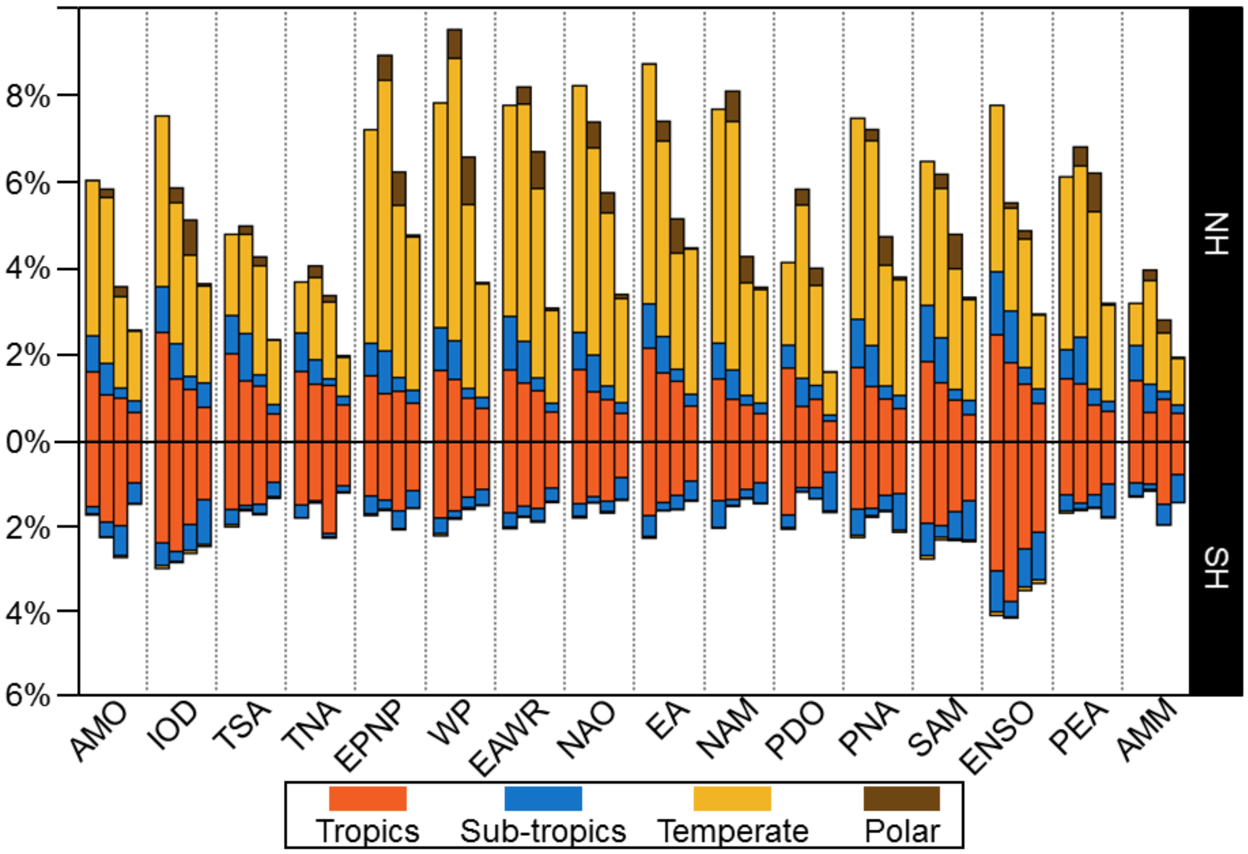

Supplementary Figure 15: Land area subject to the influence of each teleconnection on terrestrial evaporation. The bars show the percentage of land area where each mode affects the variability in terrestrial evaporation (i.e. the oscillation has a regression coefficient > 0 in the LASSO model) and are coloured for different latitudinal regions: tropics (0–23.5°), sub-tropics (23.5–35°), temperate (35–66.6°), and polar (66.5-90°). Percentages are calculated relative to the total land area, excluding pixels with missing data (e.g. in high latitudes during winter). Importance ranking is based on the magnitude of the regression coefficients from the resulting LASSO model targeting the anomalies of terrestrial evaporation based on the CIs (Supplementary Figures 1–4). Only statistically significant (*p* < 0.05) models are considered. Results are shown from left to right for DJF, MAM, JJA, and SON. Modes of climate variability are ranked in this plot according to the average dominance over all seasons.

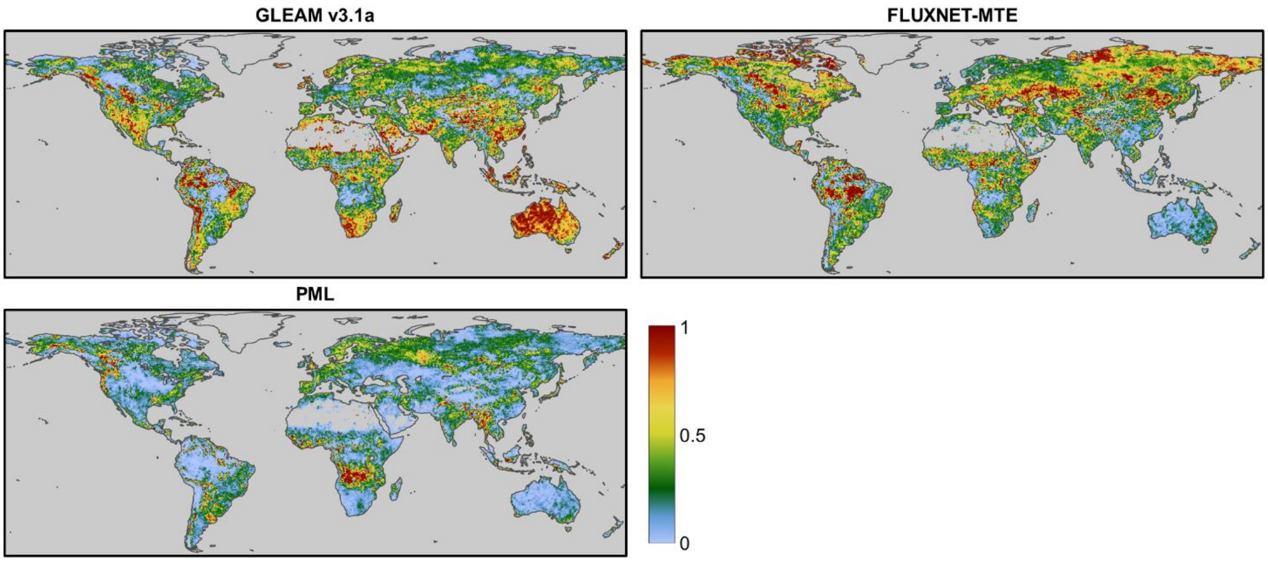

Supplementary Figure 16: Weights attributed to each of the datasets of terrestrial evaporation in the merging. Weights are calculated using the inverse variance technique, where the variance of the respective error distributions is estimated using a Triple Collocation Analysis [5].

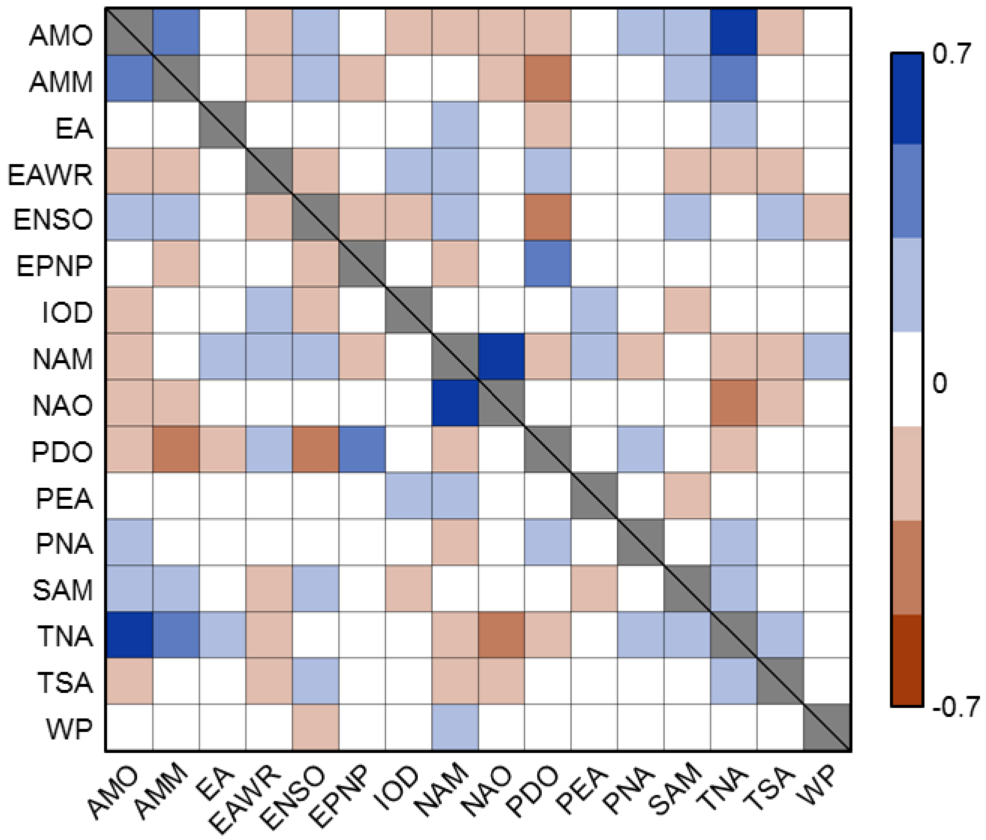

Supplementary Figure 17: Pearson correlation matrix of the 16 selected CIs. Statistically non-significant correlations (*p* > 0.05) – calculated using a two-sided Student's *t*-test – are set to zero, and the diagonal values are masked.

3. SUPPLEMENTARY REFERENCES

1. Martens, B. et al. GLEAM v3: satellite-based land evaporation and root-zone soil moisture. Geosci. Model. Dev. 10, 1903–1925 (2017).
2. Miralles, D. G. et al. Global land-surface evaporation estimated from satellite-based observations. Hydrol. Earth Syst. Sci. 15, 453–469 (2011).
3. Zhang, Y. et al. Multi-decadal trends in global terrestrial evapotranspiration and its components. Sci. Rep. 6, 19124 (2016).
4. Jung, M., Reichstein, M. & Bondeau, A. Towards global empirical upscaling of FLUXNET eddy covariance observations: validation of a model tree ensemble approach using a biosphere model. Biogeosciences Discuss. 6, 5271–5304 (2009).
5. Jung, M. et al. Global patterns of land-atmosphere fluxes of carbon dioxide, latent heat, and sensible heat derived from eddy covariance, satellite, and meteorological observations. J. Geophys. Res. Biogeosciences 116, 1–16 (2011).

6. Scipal, K. et al. A possible solution for the problem of estimating the error structure of global soil moisture data sets. Geophys. Res. Lett., 35 (2008).